This article has been accepted for publication in a future issue of this journal, but has not been fully edited. Content may change prior to final publication. Citation information: DOI 10.1109/JPHOT.2019.2936485, IEEE Photonics Journal

Fano-like resonance in an all-in-fiber structure

Biqiang Jiang,[1,2] Xuetao Gan,[1] Linpeng Gu,[1] Zhen Hao,[1] Shouheng Wang,[1] Zhixuan Bi,[1] Lin Zhang,[2] Kaiming Zhou,[1,2] and Jianlin Zhao[1]

[1]MOE Key Laboratory of Material Physics and Chemistry Under Extraordinary Conditions and Shaanxi Key Laboratory of Optical Information Technology, School of Science, Northwestern Polytechnical University, Xi'an 710072, China
[2]Aston Institute of Photonic Technologies, Aston University, Birmingham B4 7ET, United Kingdom
[3]State Key Laboratory of Transient Optics and Photonics, Xi'an Institute of Optics and Precision Mechanics, Chinese Academy of Sciences, Xi'an 710119, China

Corresponding authors: Xuetao Gan; Jianlin Zhao (e-mail: xuetaogan@nwpu.edu.cn; jlzhao@nwpu.edu.cn).

Abstract: We achieve Fano-like resonances in an all-in-fiber structure embedded with an in-line Mach-Zehnder interferometer (MZI). A fiber Bragg grating is inserted into MZI's one arm to form a resonance, which functions as the discrete state of the Fano-like resonance to couple with the continuum propagating mode of MZI in the fiber core. A theoretical model predicts the controllable resonance lineshape by changing the phase difference between the MZI's two interference pathways. Fano-like resonances with an extinction ratio over 20 dB are experimentally observed, which are reliably tuned into Lorentzian and electromagnetically induced transparency-like resonances by versatile methods. The realization of Fano-like resonances with broad tunability in this all-in-fiber structure holds potentials in fiber-based applications of sensing, signal processing and nonlinear optics.

Index Terms: Fano-like resonance, fiber Bragg grating (FBG), Mach-Zehnder interferometer (MZI).

1. Introduction

Recently, Fano-like resonances in photonic structures have attracted great research interests. Comparing with conventional Lorentzian resonances, Fano-like resonances have asymmetric lineshapes [1], which therefore provide good potential for controlling the propagation velocity of light [2, 3], lowering the power threshold of optical switching [4], and enhancing the sensitivity of optical sensing [5]. Similar to those defined in the quantum systems [6, 7], Fano-like resonances in optical systems are realized by interfering a discrete resonance state with a continuum of states. And electromagnetically induced transparency (EIT) is a result of Fano interference that requires coupling of a discrete transition to a continuum, creating a narrow transparency window due to elimination of the resonant absorption [8]. A variety of optical microresonators with narrow resonance linewidths such as chip-integrated microrings and microtoroids [9], individual microspheres [10], and microbottles [1, 11] , have been coupled with interferometers of wide spectrum to form Fano-like resonance lineshapes. However, to access resonant modes in these microresonators, tapered microfibers or lensed fibers are essential, which make the coupling configurations rigorous and require the strict coupling gap and phase matching condition [12, 13]. For instance, coupling with a microtoroid requires the microfiber to have waist diameters smaller than 2 μm [10-12, 14], and the coupling efficiency strongly depends on their coupling gap. It is a challenge to package these fibers and micro cavities into a compact system. In addition, the fabrication processes for microcavities and microfibers are complicated.

Realizing an all-in-fiber arrangement for Fano-like resonance would be attractive for solving these problems. Here, we propose a fiber structure with an in-line Mach-Zehnder interferometer (MZI) to implement the realizations of Fano-like resonances. The two arms of the MZI are the core mode and cladding modes propagating in a D-shaped fiber, respectively. An optical cavity is formed in one arm of the MZI by inserting a fiber Bragg grating (FBG). Because of the easy tunability of the in-line MZI and FBG, the resonance lineshapes could be tuned into Lorentzian or EIT-like resonance lineshapes via bending and twisting. Experimental results verify the theoretical analysis well and represent a Fano-like resonance lineshape with an extinction ratio of over 20 dB and a slope rate about 32.6 dB/nm. Compared with other reported devices, the proposed in-line fiber structure has no tapered microfiber and separated microresonators. It is robust, compact, of easy fabrication, and broad tunability, showing great potentials to be employed in fiber-based applications, including sensing, signal processing, nonlinear optics, etc.

2. Theoretical model for all-in-fiber Fano-like resonances

A theoretical model was built to study the generation and features of Fano-like resonances in the proposed structure, as schematically depicted in Fig. 1(a). An in-line fiber MZI was constructed by splicing a short segment of single fiber with slightly misaligned fiber core. An FBG is inscribed into the short fiber segment. The two splicing joints of the MZIs act as the beam splitter and beam combiner, respectively. The input light, with an electric component $\boldsymbol{E}_0$ is divided into the core mode $\boldsymbol{E}_1$ and cladding modes $\boldsymbol{E}_2$ at the first splicing joint, and then mixed at the second joint and partly coupled back to the core of the lead-out SMF, forming the output light $\boldsymbol{E}_3$. The propagating core mode $\boldsymbol{E}_1$ will be reflected by the inscribed FBG at the distributed Bragg reflection wavelength. For the sake of simplicity, we assuming a splitting ratio of 50:50 at the splicing joint.

This article has been accepted for publication in a future issue of this journal, but has not been fully edited. Content may change prior to final publication. Citation information: DOI 10.1109/JPHOT.2019.2936485, IEEE Photonics Journal

And the transmissivities of the splicing joint and FBG are t_s and t_{FBG}, respectively, then the reflectivity of the FBG is 1-t_{FBG}, as shown in Fig. 1(a). The total transmission of the whole in-line MZI can be expressed as

$$T=\left|\frac{\boldsymbol{E}_3}{\boldsymbol{E}_0}\right|^2=\frac{1}{4}\left[\left(t_s t_{FBG} t_s\right)^2+1+2\left(t_s t_{FBG} t_s\right)\cos\left(\Delta\varphi_s+\Delta\varphi_{FBG}+\Delta\varphi_{MZI}+\Delta\varphi_e\right)\right]. \quad (1)$$

Where, $\Delta\varphi_{FBG}$ and $\Delta\varphi_s$ are the phase shift induced by the FBG and two splicing joints, respectively, $\Delta\varphi_{MZI}=2\pi\Delta n_{eff}(\lambda)L_D/\lambda$ is the initial static phase difference accumulated between the MZI's two interference pathways, depending on the propagating distance L_D, the effective refractive index (RI) difference Δn_{eff} between the two pathways, and the light wavelength λ. Additionally, an extra phase delay $\Delta\varphi_e$ can be introduced by bending, heating or twisting the device, to adjust the position of the interference dip of the MZI.

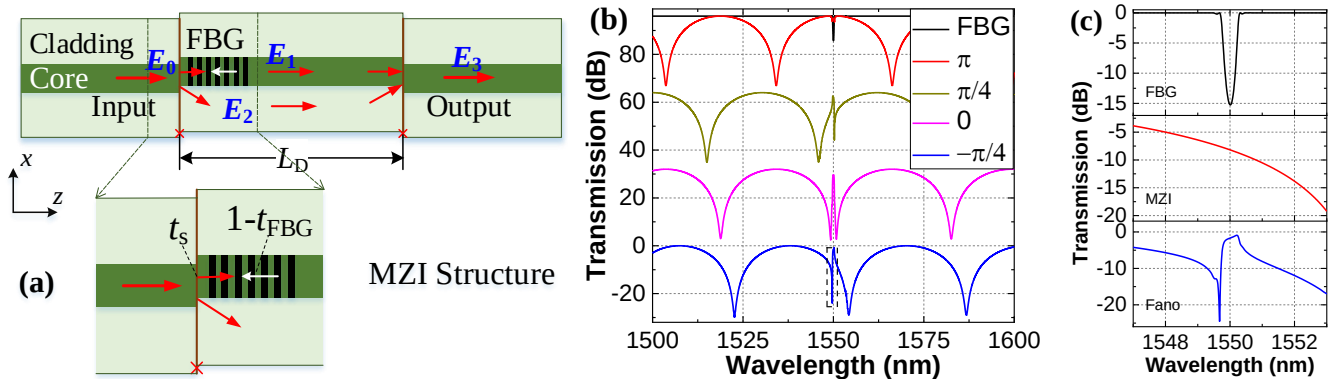

Fig.1. (a) Schematic diagram of an in-line MZI embedded with a FBG, indicating the propagation of the input light. (b) Transmission spectra of the individual FBG, MZI and their coupling structures with different phase shifts $\Delta\varphi_e$ of π, π/4, 0, and -π/4. For clarity, the spectra are shifted vertically. (c) Zoomed spectra of FBG, MZI and the corresponding Fano-like resonance in the dashed region of (b) at the phase shift $\Delta\varphi_e$ of -π/4.

To obtain further insight, we numerically solved Eq. (1) by using the transfer matrix method to disclose the generation and tunability properties of the Fano-like resonances. Transmission spectra of the individual FBG and MZI are plotted in the top curve of Fig. 1(b). In the simulation, the transfer matrix T_s of the splicing joint is determined as [4]

$$T_s=\frac{1}{i\sqrt{1-r^2}}\begin{bmatrix}-1 & -r\\ r & 1\end{bmatrix}, \quad (2)$$

where r is the amplitude reflectivity of the splicing joint, and then the transmissivity $t_s=\sqrt{1-r^2}$. The generation of Fano-like resonance is independent of the transmissivity, but will affect the visibility of MZI and then the extinction ratio of Fano-like lineshape. Here, the r value is set as 0.05 for high visibility (~30 dB) of MZI. The employed FBG is apodized with a super-Gaussian profile $g(z)=A\times\exp[-G\times(z/L)^4]$ for calculating the spectrum. Where, A and G are the constants in the Gaussian function, z and L is the grating position and total length. Actually, the apodization of FBG can effectively eliminate the sidelobes and ripples in the Fano-like resonance spectrum. For the apodized FBG, the transfer matrix T_{FBG} of the FBG is given by the previous report in [15]. Therefore, the transfer matrix T for the entire device is determined by T_s, T_{FBG}, and the phase delay matrix in the fiber core excluding FBG section. Fig. 1(c) gives the zoomed spectra of the FBG, MZI and then inducing Fano-like resonance. We can observe the Fano-like lineshape, resulting from the coupling interaction between the Bragg resonance in the FBG and the continuum propagating mode of MZI in the fiber core. Also from Fig. 1(c), we use an approximately Lorentzian lineshape to describe the symmetric spectrum of the FBG, which is just for comparison to the asymmetric Fano-like lineshape. The transmission spectrum of 15mm long MZI has a period of around 31.3nm.

The change of $\Delta\varphi_e$ will lead to a global spectrum shift of the MZI, which couples with the FBG will give various lineshapes at the FBG wavelength. When $\Delta\varphi_e=\pi$, the MZI transmission has a peak at the FBG wavelength, and a Lorentzian transmission dip superimposes over it. By changing $\Delta\varphi_e$ to π/4, the spectrum lineshape at FBG wavelength evolves from a symmetric dip into an asymmetric peak, and further converts to a symmetric EIT-like peak when $\Delta\varphi_e=0$. When $\Delta\varphi_e$ is changed to -π/4, the sharply asymmetric Fano-like lineshape appears again.

For the FBG embedded in the MZI, the contribution of the FBG on the Fano-like resonance is significant when the resonant dip of MZI is close to the Bragg wavelength λ_B, due to strong contra-propagating coupling of the core mode. We can therefore observe sharply asymmetric Fano-like lineshapes in Fig. 1(b), resulting from the coupling between the MZI and Bragg resonance formed by FBG. In view of this mechanism, the formed Fano-like resonance lineshape depends critically on the resonant wavelength of the MZI dips determined by the extra phase shift $\Delta\varphi_e$.

3. Device fabrication

In-line MZI structures are compact, robust and of easy fabrication, and usually involve two fiber mode-coupling joints. For instance, the MZIs consisting of up-tapers or lateral-offsets or peanut-shape structures [16, 17], or employing

This article has been accepted for publication in a future issue of this journal, but has not been fully edited. Content may change prior to final publication. Citation information: DOI 10.1109/JPHOT.2019.2936485, IEEE Photonics Journal

single-mode/multi-mode/single-mode (SMS) or twin-core fiber structures [18, 19] have been implemented to achieve the intermodal interference. Here, we inserted a small segment of asymmetrical D-shaped fiber to construct the MZI, as shown in Fig. 2(a), which promises sensitive wavelength responses and broader tuning on the mechanical strain, bending and temperature [20]. The inset shows the cross-section of the employed D-shaped fiber with the asymmetric structure, the fiber core with a diameter of 9.57 μm is placed at a distance of 3.55 μm from the flat surface. In the splicing process, a polarization-maintaining (PM) fiber arc fusion splicer was employed to fabricate the MZI with D-shaped fiber, and then the offset, arc power/time and other splicing parameters can be precisely controlled by the splicer program. In particular, the orientation of flat surface of D-shaped fiber is also adjusted by rotating θ-axis motor of the splicer.

The prepared MZI structure was firstly hydrogenated for photosensitivity enhancement, and then a FBG was UV-inscribed into the D-shaped fiber by using the scanning phase-mask technique and a frequency-doubled continuous wave argon-ion laser [20, 21]. During the inscription, the flat surface of D-shaped fiber is rotated to face the phase mask and UV-laser, avoiding the asymmetric edge diffraction for an improvement of the inscription efficiency. The lengths of D-shaped fiber and inscribed FBG are 15mm and 5mm, respectively, and the FBG is close to the first splicing joint. Light from a broadband supercontinuum (superK) source is launched into the fabricated device, and its transmission spectra are monitored by an optical spectrum analyzer (OSA).

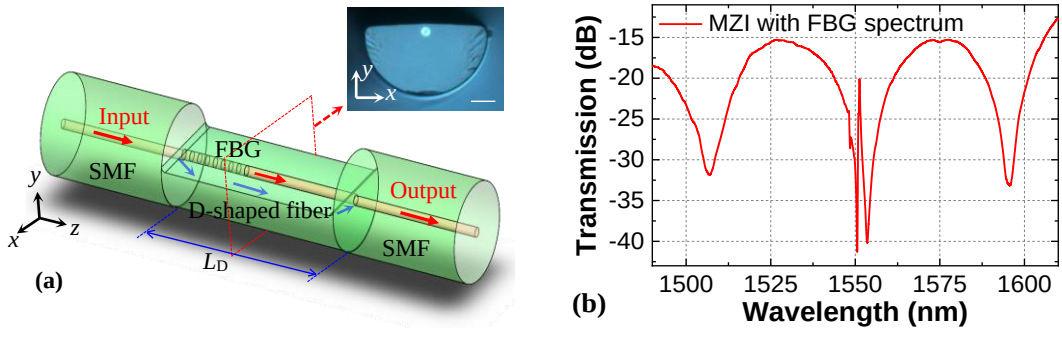

Fig. 2. (a) Schematic diagram of the fabricated device for generating the Fano-like resonance. The inset is the cross-section image of the D-shaped fiber, and the scale bar is 25 μm. (b) Measured transmission spectrum of the device.

Figure 2(b) displays the measured transmission spectrum. We can clearly observe MZI's periodical interference dips with good visibility of >15 dB and a free spectral range (FSR) of 44.38 nm in the range of 1490~1610 nm, and a sharply asymmetric Fano-like lineshape with an extinction ratio of over 20 dB and a slope rate about 32.6 dB/nm. The extinction ratio and slope rate represent the difference and steepness between the peak and dip of Fano-like resonance spectrum, and they are key parameters for Fano resonance in many applications [22-25]. Based on above simulation results, when we introduced an extra phase delay by the artificial factors, making the resonant dip of MZI close to or far away from the resonant wavelength of FBG, then the lineshape of FBG resonance will convert to the other Fano-like and EIT-like lineshapes.

4. Experimental demonstration and tuning of the Fano-like resonance

The fabricated in-line fiber device allows different methods to tune the Lorentzian lineshape to Fano-like, even to EIT-like lineshape, such as heating, bending, or twisting the device. The total phase difference $\Delta\varphi$ (sum of the phase shifts $\Delta\varphi_{MZI}$, $\Delta\varphi_{FBG}$, $\Delta\varphi_S$ and $\Delta\varphi_e$) between the interference pathways determines the resonant wavelengths of the MZI, and $\Delta\varphi=(2m+1)\pi$ satisfies the condition of destructive interference to form a transmission dip, where m is the order of the MZI. The wavelength λ_m of the destructive interference dips can therefore be found at [26]

$$\lambda_m = \frac{2\Delta n_{\text{eff}} L_D}{2m+1}. \tag{2}$$

The changes of Δn_{eff} and L_D will result in the shift of the resonant dips of MZI. From Eq. (2), the FSR can be approximated as $\Delta\lambda_m=4\Delta n_{\text{eff}}L_D/[(2m+1)(2m-1)]\approx\lambda_m^2/(\Delta n_{\text{eff}}L_D)$, and the FSR is inversely proportional to the L_D and Δn_{eff}.

According to FBG's resonant wavelength $\lambda_G=2n_{\text{eff}}\Lambda$ and Eq. (2), with the heating, twisting, especially bending of the D-shaped section of the device, the total phase shift $\Delta\varphi$ will be modulated as well as the transmission dips of MZI and FBG wavelengths. Drawing on the bending measurement principles from our previous work [20], the shift of resonant dips of the MZI linearly depends on the curvature change ΔC as

$$\Delta\lambda_{\text{MZI}} \cong \frac{2kL_D d}{2m+1}\cdot\Delta C, \tag{3}$$

where d is the distance between the fiber core and cladding, and k is the strain-RI coefficient. Due to the asymmetric

This article has been accepted for publication in a future issue of this journal, but has not been fully edited. Content may change prior to final publication. Citation information: DOI 10.1109/JPHOT.2019.2936485, IEEE Photonics Journal

structure of D-shaped fiber, the behavior of wavelength shift is also dependent of the bending orientations.

To change the curvature, the device was placed to form a simply-supported beam shown in [20]. By bending the device along the *x*-axis, the curvature was calculated by the equation $C=2y/(y^2+L^2)$, where *y* is the displacement of the center of the fiber beam, and *L* is one half of the fiber beam length. We obtained the evolution of transmission spectra of the device with the curvature ranging from 0 to 0.3m^{-1}, as shown in Fig. 3. The four spectra correspond to the cases with the curvatures of 0, 0.1 m^{-1}, 0.2 m^{-1}, and 0.3 m^{-1}, respectively. Since the FBG is almost located in the neutral surface of D-shaped fiber, the bending only yields the shift of the resonant dips of MZI. For the unbent D-shaped fiber, the MZI presents a constructive interference peak at Bragg wavelength of FBG, resulting in a normal Bragg resonance and then a symmetric Lorentzian-shape resonant dip. As the applied curvature increases to 0.1 m^{-1}, the MZI interference blue-shifts, and the FBG's resonant dip evolves into a Fano-like lineshape with a sharp rising slope. If the curvature further increases to 0.2 m^{-1}, the destructive interference dip of MZI coincides with the resonant wavelength of FBG. Then, the superposed signal of the FBG and MZI converts into an EIT-like lineshape, where a sharp "transparency window" exhibits at the Bragg resonance overlapping the wide interference fringe [8, 27], as displayed in Fig. 3. Compared with WGM-based structures [1, 10], there is a more prominent EIT-like spectrum, and the height of the transparency peak is up to ~10.2 dB (shown in Fig. 3). When the curvature is larger than 0.2 m^{-1}, Fano-like resonance appears again. When the curvature increases to 0.3 m^{-1}, the asymmetric lineshape has a sharp falling slope, which is different from the case of 0.1 m^{-1} curvature. The above experimental observations indicate that the lineshape of the resonance depends critically on the position of the Bragg wavelength with respect to the MZI interference dip considering the coupling between the MZI resonance and the FBG-induced FP-type resonance. The lineshape can therefore be switched among the Lorentzian, Fano, and EIT types, which agrees well with theoretical results shown in Fig. 1(b).

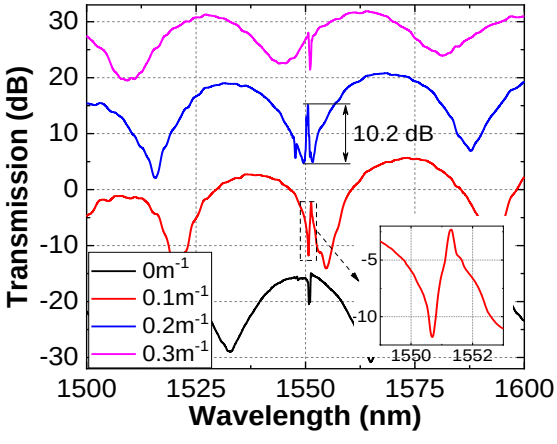

Fig. 3. Experimentally measured transmission spectra by bending the device for different values of the curvatures when at a torsional angle of 0°. For clarity, the spectra are shifted vertically.

We can also twist the proposed device to implement the tuning of the Fano-like lineshape, by exploiting of that the resonances of MZI and FBG wavelength have difference responses to the torsion. The two pigtails of the device were mounted on two fiber rotators for twisting the 15cm fiber device, and the fiber was kept straight to eliminate any bending effects. We rotated one of the two rotators to twist the device, and the torsional angle can be measured by the rotator. When the device was rotated from 0° to 180° with an increment of 30°, we obtained the transmission spectra of the fabricated device at different torsional angles, as shown in Fig. 4(a). We can clearly observe that one of the resonant dips of the MZI moves towards the Bragg resonance of the FBG, and then the Fano-like resonance grows to EIT-like resonance while the MZI's resonant dip gradually fades away with the torsional angle changed from 0° to 180°. As shown in Fig. 4(b), during the twisting, the wavelength of the Fano-like resonance keeps almost unchanged since the FBG always located in the neutral axis, but the MZI's resonant dip blue-shifts, resulting from twist-induced extra phase delay. By tracking the Dip A (marked in Fig. 4(a)) of the MZI resonance, its twisting response coefficient is ~79.94pm/°.

This article has been accepted for publication in a future issue of this journal, but has not been fully edited. Content may change prior to final publication. Citation information: DOI 10.1109/JPHOT.2019.2936485, IEEE Photonics Journal

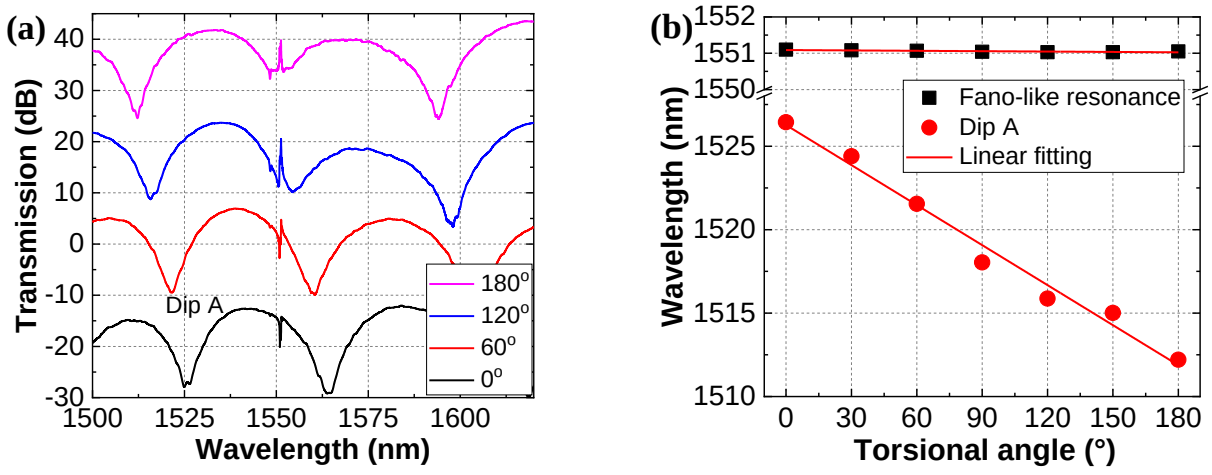

Fig. 4. (a) Experimentally measured transmission spectra by twisting the device for different torsional angles at a bending curvature of 0 m^{-1}. For clarity, the spectra are shifted vertically. (b) Torsion response of the sharp Fano-like resonance and the Dip A.

5. Conclusions

We have constructed an in-line fiber structure to achieve a tunable Fano-like resonance lineshape by inserting a FBG in the MZI. In the theoretical analysis, we found the sharp asymmetric Fano-like lineshape appears when the Bragg wavelength of FBG locates in both side-shoulders of the interference of the MZI. Also, the lineshape strongly depends on the induced extra phase delay $\Delta\varphi_e$, which determines the relative position of the resonances of MZI and FBG wavelength. In the experiment, we achieved the tuning of the Fano-like resonance and switched it among the Lorentzian, Fano, and EIT types by bending and twisting the device. Compared with other Fano-like resonance schemes achieved in photonic structures [1, 9-11], the proposed scheme can generate Fano-like resonance with only an in-line fiber structure, enabling a compact, stable and robust device. By merging the advantages of all-in-fiber device, this hybrid structure with fiber interferometer and grating shows great promises for Fano-like resonance based signal processing, multi-parameter measurement simultaneously, etc.

Acknowledgements

This work was supported by the National Natural Science Foundation of China (Grant Nos. 61775182, 61505165, and 61522507), the Natural Science Basic Research Plan in Shaanxi Province of China (Grant No. 2019JM-330), the Fundamental Research Funds for the Central Universities (Grant No. 3102019PB005), the Key Laboratory of Opto-electronic Information Technology, Ministry of Education (Tianjin University) (Grant No. 2019KFKT007), and the Marie Skłodowska-Curie Individual Fellowships in the European Union's Horizon 2020 Research and Innovation Programme (Grant No. 660648).

References

[1] K. Zhang, Y. Wang, and Y.-H. Wu, "Enhanced Fano resonance in a non-adiabatic tapered fiber coupled with a microresonator," *Opt. Lett.,* vol. 42, no. 15, pp. 2956-2959, 2017.
[2] K. Totsuka, N. Kobayashi, and M. Tomita, "Slow light in coupled-resonator-induced transparency," *Phys. Rev. Lett.,* vol. 98, no. 21, pp. 213904, 2007.
[3] Y.-F. Xiao, X.-B. Zou, W. Jiang, Y.-L. Chen, and G.-C. Guo, "Analog to multiple electromagnetically induced transparency in all-optical drop-filter systems," *Phys. Rev. A,* vol. 75, no. 6, pp. 063833, 2007.
[4] S. Fan, "Sharp asymmetric line shapes in side-coupled waveguide-cavity systems," *Appl. Phys. Lett.,* vol. 80, no. 6, pp. 908-910, 2002.
[5] W. Qiu, A. Ndao, V. C. Vila, R. Salut, N. Courjal, F. I. Baida, and M.-P. Bernal, "Fano resonance-based highly sensitive, compact temperature sensor on thin film lithium niobate," *Opt. Lett.,* vol. 41, no. 6, pp. 1106-1109, 2016.
[6] U. Fano, "Effects of configuration interaction on intensities and phase shifts," *Phys. Rev.,* vol. 124, no. 6, pp. 1866-1878, 1961.
[7] A. E. Miroshnichenko, S. Flach, and Y. S. Kivshar, "Fano resonances in nanoscale structures," *Rev. Mod. Phys.,* vol. 82, no. 3, pp. 2257-2298, 2010.
[8] B. Peng, Ş. K. Özdemir, W. Chen, F. Nori, and L. Yang, "What is and what is not electromagnetically induced transparency in whispering-gallery microcavities," *Nat. Commun.,* vol. 5, pp. 5082, 2014.
[9] F. Lei, B. Peng, Ş. K. Özdemir, G. L. Long, and L. Yang, "Dynamic Fano-like resonances in erbium-doped whispering-gallery-mode microresonators," *Appl. Phys. Lett.,* vol. 105, no. 10, pp. 101112, 2014.
[10] C. Zhao, X. Gan, L. Fang, L. Han, K. Chang, D. Li, and J. Zhao, "Tunable Fano-like resonance enabled by coupling a microsphere with a fiber Mach-Zehnder interferometer," *Appl. Opt.,* vol. 55, no. 21, pp. 5756-5760, 2016.
[11] Z. Chenari, H. Latifi, O. R. Ranjbar-Naeini, M. I. Zibaii, E. Behroodi, and A. Asadollahi, "Tunable Fano-like lineshape in an adiabatic tapered fiber coupled to a hollow bottle microresonator," *J. Lightwave Technol.,* vol. 36, no. 3, pp. 735-741, 2018.
[12] J. C. Knight, G. Cheung, F. Jacques, and T. A. Birks, "Phase-matched excitation of whispering-gallery-mode resonances by a fiber taper," *Opt. Lett.,* vol. 22, no. 15, pp. 1129-1131, 1997.
[13] B. Li, Y. Xiao, C. Zou, Y. Liu, X. Jiang, Y. Chen, Y. Li, and Q. Gong, "Experimental observation of Fano resonance in a single whispering-gallery microresonator," *Appl. Phys. Lett.,* vol. 98, no. 2, pp. 021116, 2011.
[14] X. Zhang, Y. Yang, H. Shao, H. Bai, F. Pang, H. Xiao, and T. Wang, "Fano resonances in cone-shaped inwall capillary based microsphere resonator," *Opt. Express,* vol. 25, no. 2, pp. 615-621, 2017.
[15] T. Erdogan, "Fiber grating spectra," *J. Lightwave Technol.,* vol. 15, no. 8, pp. 1277-1294, 1997.

[16] B. Sun, Y. Huang, S. Liu, C. Wang, J. He, C. Liao, G. Yin, J. Zhao, Y. Liu, J. Tang, J. Zhou, and Y. Wang, "Asymmetrical in-fiber Mach-Zehnder interferometer for curvature measurement," *Opt. Express,* vol. 23, no. 11, pp. 14596-14602, 2015.
[17] H. Gong, M. Xiong, Z. Qian, C. L. Zhao, and X. Dong, "Simultaneous measurement of curvature and temperature based on Mach-Zehnder interferometer comprising core-offset and spherical-shape structures," *IEEE Photon. J.,* vol. 8, no. 1, pp. 1-9, 2016.
[18] W. Ni, P. Lu, J. Zhang, C. Yang, X. Fu, Y. Sun, H. Liao, and D. Liu, "Single hole twin eccentric core fiber sensor based on anti-resonant effect combined with inline Mach-Zehnder interferometer," *Opt. Express,* vol. 25, no. 11, pp. 12372-12380, 2017.
[19] Q. Wu, Y. Semenova, P. Wang, and G. Farrell, "High sensitivity SMS fiber structure based refractometer – analysis and experiment," *Opt. Express,* vol. 19, no. 9, pp. 7937-7944, 2011.
[20] B. Jiang, Z. Bai, C. Wang, Y. Zhao, J. Zhao, L. Zhang, and K. Zhou, "In-line Mach-Zehnder interferometer with D-shaped fiber grating for temperature-discriminated directional curvature measurement," *J. Lightwave Technol.,* vol. 36, no. 3, pp. 742-747, 2018.
[21] B. Jiang, K. Zhou, C. Wang, Q. Sun, G. Yin, Z. Tai, K. Wilson, J. Zhao, and L. Zhang, "Label-free glucose biosensor based on enzymatic graphene oxide-functionalized tilted fiber grating," *Sens. Actuators B Chem.,* vol. 254, pp. 1033-1039, 2018.
[22] X. Liu, Y. Yu, and X. Zhang, "Tunable Fano resonance with a high slope rate in a microring-resonator-coupled Mach–Zehnder interferometer," *Opt. Lett.,* vol. 44, no. 2, pp. 251-254, 2019.
[23] W. Lin, H. Zhang, S.-C. Chen, B. Liu, and Y.-G. Liu, "Microstructured optical fiber for multichannel sensing based on Fano resonance of the whispering gallery modes," *Opt. Express,* vol. 25, no. 2, pp. 994-1004, 2017.
[24] G. Dong, Y. Wang, and X. Zhang, "High-contrast and low-power all-optical switch using Fano resonance based on a silicon nanobeam cavity," *Opt. Lett.,* vol. 43, no. 24, pp. 5977-5980, 2018.
[25] B. Luk'yanchuk, N. I. Zheludev, S. A. Maier, N. J. Halas, P. Nordlander, H. Giessen, and C. T. Chong, "The Fano resonance in plasmonic nanostructures and metamaterials," *Nat. Mater.,* vol. 9, pp. 707, 2010.
[26] Z. Li, C. Liao, D. Chen, J. Song, W. Jin, G.-D. Peng, F. Zhu, Y. Wang, J. He, and Y. Wang, "Label-free detection of bovine serum albumin based on an in-fiber Mach-Zehnder interferometric biosensor," *Opt. Express,* vol. 25, no. 15, pp. 17105-17113, 2017.
[27] Q. Xu, S. Sandhu, M. L. Povinelli, J. Shakya, S. Fan, and M. Lipson, "Experimental realization of an on-chip all-optical analogue to electromagnetically induced transparency," *Phys. Rev. Lett.,* vol. 96, no. 12, pp. 123901, 2006.